Sea surface source-side static optimization for 4D seismic

Simon R. Barnes, Paul Lecocq and Stephane Perrier, PGS and Mick Igoe, Tullow Oil*

Summary

Management of producing fields can be enhanced by effective seismic reservoir monitoring. Improved repeatability of 4D monitor surveys can be achieved by applying deghosting and datuming via seismic wavefield separation. By also correcting for the variable distance of the source above the seabed caused by the sea state will increase 4D repeatability further.

Introduction

One of the key challenges of 4D seismic reservoir monitoring is to maximize the repeatability of successive towed streamer surveys. Using dual-sensor streamer technology and associated seismic wavefield separation, the effect of the sea state can be more or less entirely removed on the receiver-side but only the ghosting related to the relative movement of the source below the sea surface on the source-side. This abstract deals with the outstanding correction for the variation of distance of the source array above the seabed (within each sail line) at the preprocessing stage that is also related to the sea state and in particular the height of a wave and its corresponding displacement at the instant the recording of a shot gather commences (Figure 1) rather than during acquisition (Goto *et al*, 2008).

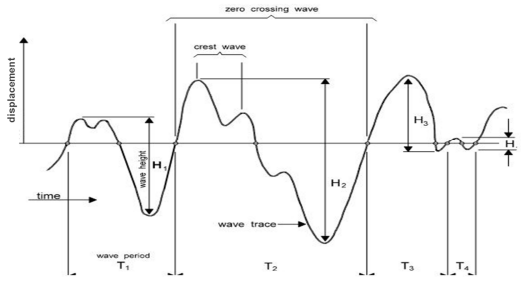

Figure 1: An individual sea wave in the time domain can be roughly defined from the time interval between two successive downward-crossings through the average surface elevation (upward-crossings might also be used) from a wave record. The individual wave height is then the difference between the maximum and minimum elevation in that time interval (after the Manly Hydraulics Laboratory website, New South Wales Government).

Sea waves are measured by a variety of methods with their associated wave energy spectra in the frequency domain now typically computed via remote sensing from satellites. In theory, if the heights and frequencies of all the contributing waves were known, we would be able to predict all the heights and frequencies of the real waves (Orji *et al*, 2010). In practice, this is rarely possible. Instead, a particular sea state is commonly characterized by a single attribute termed the significant wave height, H_s, a reference average height of the highest one-third of all sea waves occurring in a particular time period (World Meterological Organization sea state code) corresponding to the 71st percentile of a Rayleigh probability function of wave heights in the time domain where the total energy being dissipated by the waves is the same as that received from the wind. As wind speed increases, so H_s and the dominant wave period increase (Figure 2). Note that the height of highest waves can be nearly twice as high as H_s.

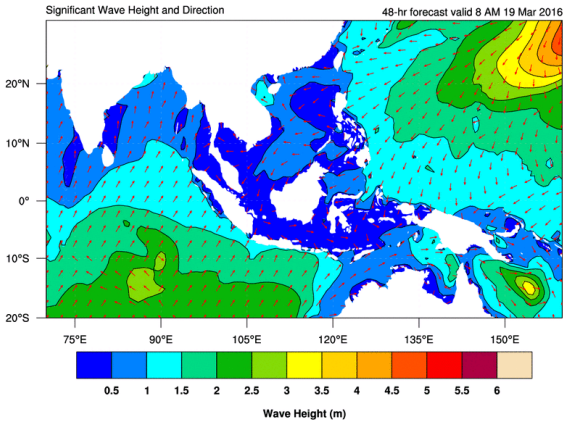

Figure 2: Predicted significant wave height in the Asia Pacific. A gale has formed in the top right corner (after the Meteorological Service Singapore website, Singapore Government).

In reality, this model of a fully developed sea can be significantly modified by waves coming into an area from elsewhere, such as swell from a storm or gale. The longer period swell seems able to pass through locally generated seas without hindrance or interaction mainly within an angle of 30° to 45° either side of the prevailing wind direction (Brown *et al*, 2006). So where the sea state is calmer, variation in the source distance above the seabed could be more sensitive to longer period swell waves, when present, rather than shorter period wind-related ones.

Outline of the approach

In order to derive the source-side static correction for each shot, a suitable inversion technique is required. Yilmaz (2001; p336-344) gives an elegant description of the classical residual statics estimation by travel time decomposition for land surveys. Unfortunately, marine

datasets are not surface consistent, nor is the recorded upgoing wavefield vertical for all input offset traces (because of the presence of a fast overburden and an overlying very slow velocity layer). Instead our first approach to this problem (Lecocq *et al*, 2014) adopted in this abstract is to constrain rather than close out any leakage that is not shot consistent and to ensure the source consistent static derivation is data driven.

The preconditioning of the input, after the required deghosting and designature, includes a robust flattening of the moveout of the seabed over offset via a trace-by-trace NMO with 3D dip moveout. The kernel of the technique is now outlined as follows and was used for the initial synthetic proof of concept (next section). The difference in linear phase between shots is determined in 2D CMP space (where the effect of structure has been corrected for), by cross-correlating the very shallow overburden with a suitable pilot or model trace (where the similarity of the method to that for land surveys mentioned above ends). We then sort back to the shot domain where any directivity effects over offset are empirically corrected for by performing a least squares linear regression of the measured time shifts for each cable. Averaging the corresponding intercepts across all the cables produces the first estimate of the source-side static for each shot. Repeating the process described above, with further adjustments to the pilot trace, closes out any remaining residuals.

Synthetic study

The sea wave displacement that needs to be corrected for at each shot can be considered a sparse sample of the wave field (of the sea) both spatially and temporally along the sail line. Although information about individual wave heights is lost, the distribution of sea wave displacements should still be Gaussian-like so the sea state could be inferred for modelling where the difference between the minimum and maximum displacements (1^{st} and 100^{th} percentiles respectively) corresponds to the maximum wave height and, by extension, the 71^{st} percentile to H_s.

A 3D ray traced-based synthetic swath was produced, for proof of concept, comprising three dual source sail lines. The model included an irregular seabed with an overall 5° dip, 45° to the direction of shooting (worst case for azimuth differences due to structure), with underlying planar events and an intervening complex one to represent an overburden. The variation in the wave displacement on the source-side was emulated by coupling together the thickness of the water layer and the depth of the receiver so that the distance of the receiver above the seabed remained unchanged (Figure 3). A receiver ghost was not generated to emulate the removal of the down going wavefield by a suitable seismic wavefield separation process. In all, 21 model combinations were produced for shots varying up to ±2m vertically about a central reference (for no wave displacement) in increments of 0.2m. Then two surveys were created by sampling the combinations in a Gaussian manner with respect to shot for each sail line: a calmer base survey (displacements up to ±0.6m for seven combinations inclusive; $H_s \approx 0.5$m), and a rougher monitor survey (up to ±2m using all 21 combinations; $H_s \approx 2.5$m).

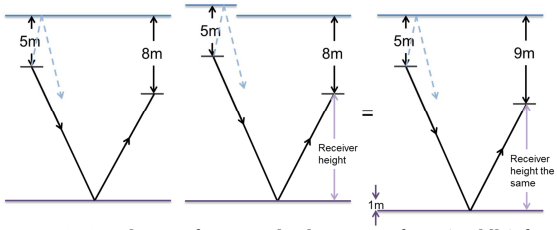

Figure 3: Simulation of a wave displacement of 1m (middle) from a reference (left) by maintaining the receiver distance above the seabed (right) as the sea surface has to be flat for ray tracing.

Profiles of the linear phase after the first iteration showed a good approximation to a line over offset (Figure 5) at the seabed. This linear-like decrease is expected as the time shift for a given shot with offset will be a function of the versine of the incident angle. Comparing the map of the computed source consistent statics (after performing three iterations of the approach described in the previous section) for the monitor survey to the modelled one (the answer) revealed a long wavelength residual (Figure 4). Although the modelled wave displacement was random, it still had a long wavelength component and this residual remained because the CMP-based cross-correlation was limited by the finite inline extent of the cable. Fortunately, a domain that still contained information of this residual was the 2D crossline space within each offset plane where both sources' contributed. The modelled traces for cross-correlating were produced by an appropriate K filtering to remove the short wavelength linear phase variation between the interleaved traces from each shot. The shot consistent static was then derived as before where it was confirmed to be long wavelength residual in the inline direction.

Field data study

The field examples are from legacy 4D baseline surveys acquired in 2007 and 2013 using a conventional survey design from the deep water Jubilee Field offshore Ghana. A comparison is made with the synthetic result after the first iteration of determining the source consistent static in the shot domain (Figure 5) and the improvement with the input after the third iteration for a NMO corrected near trace gather (Figure 7). A standard error profile is shown in Figure 6.

Conclusions

A technique to derive the source-side sea surface-related static for deeper water 4D marine datasets is proposed. The method assumes that appropriate seismic wavefield separation deghosting has been applied first. The correction for the wave displacement would be applied before a correction for water column-related statics. The method is simple and robust and the statistical standard error can be produced for quantitative analysis.

Acknowledgments

The authors would like to thank GNPC and the government of Ghana, Tullow Oil, Kosmos Energy Anadarko Petroleum and PetroSA for allowing us to present this work. A special thanks to Silke Bude (PGS Geoscience & Engineering department) for preparing the 3D synthetic. Also thanks to the PGS Imaging team in Weybridge including David Raistrick, Andrew Oates, James Owen, Paolo Paradisi and Stewart Reevell.

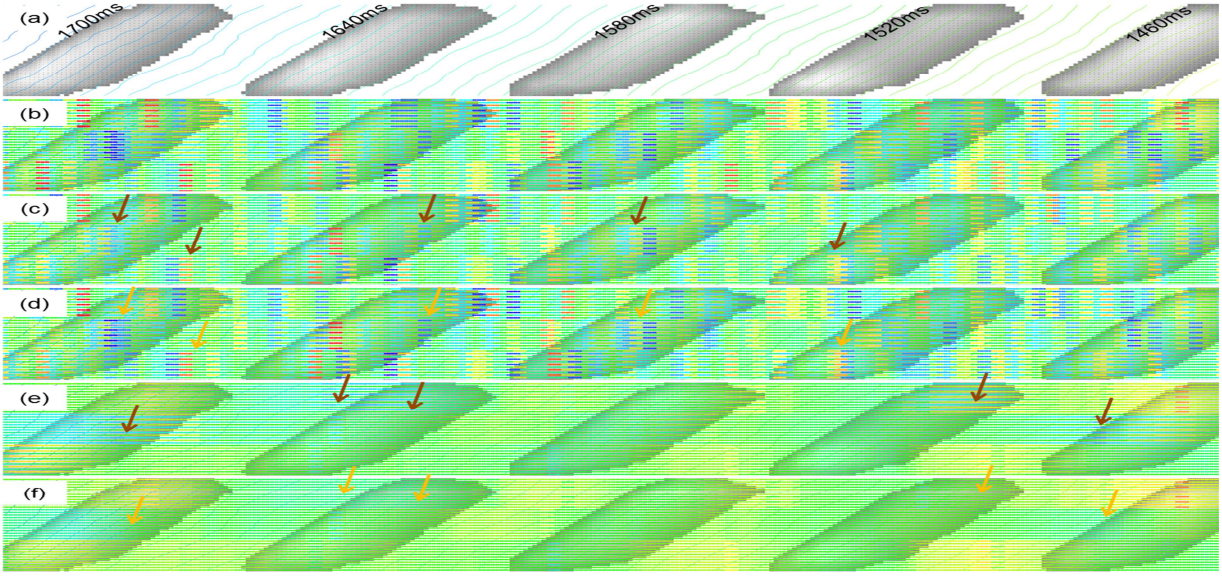

Figure 4: Near offset plane display. Monitor survey for H_s ≈2.5m. (a) Undulating seabed with local dip greater than 5° displayed in grey. Two-way time annotated. (b) Modelled source-side static. (c) Computed source-side static after one iteration. (d) Computed source-side static after three iterations. (e) Difference: (b) – (d) two times exaggeration. (f) Difference from (b) after computed crossline-based source-side static. For (b) to (d) green represents the range: -0.5ms to 0.5ms, red: -1.2ms, blue: 1.2ms.

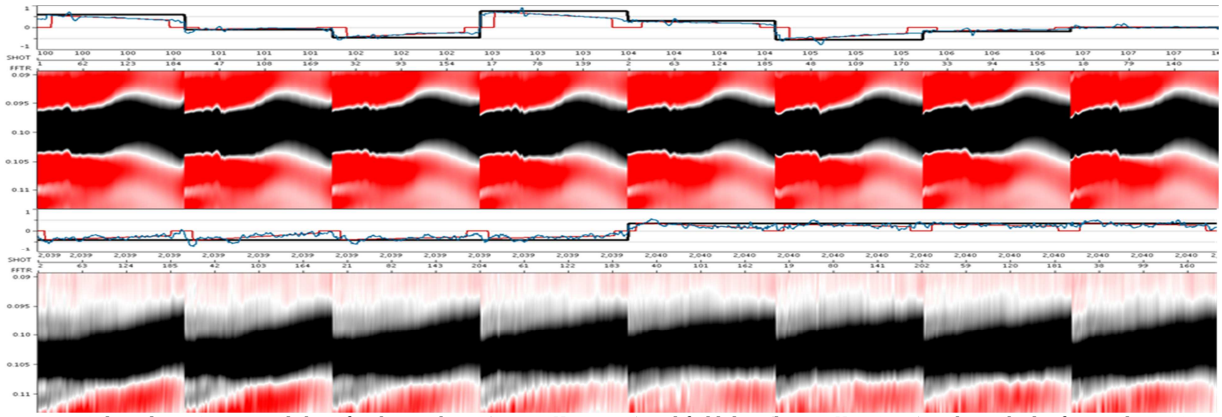

Figure 5: Selected NMO corrected shots for the synthetic (upper; H_s ≈2.5m) and field data (lower; H_s ≈0.5m) at the seabed referenced to 100ms. Profiles of linear phase (blue), best fitted straight line (red) and mean of intercepts for all cables (black) for the first iteration. Central cable only shown for the synthetic. The outer adjacent port cables of a starboard shot to the left and the corresponding starboard cables of the next port shot to the right shown for the 2013 field data. The 12 estimates from all the cables for each shot are used to determine the standard mean error.

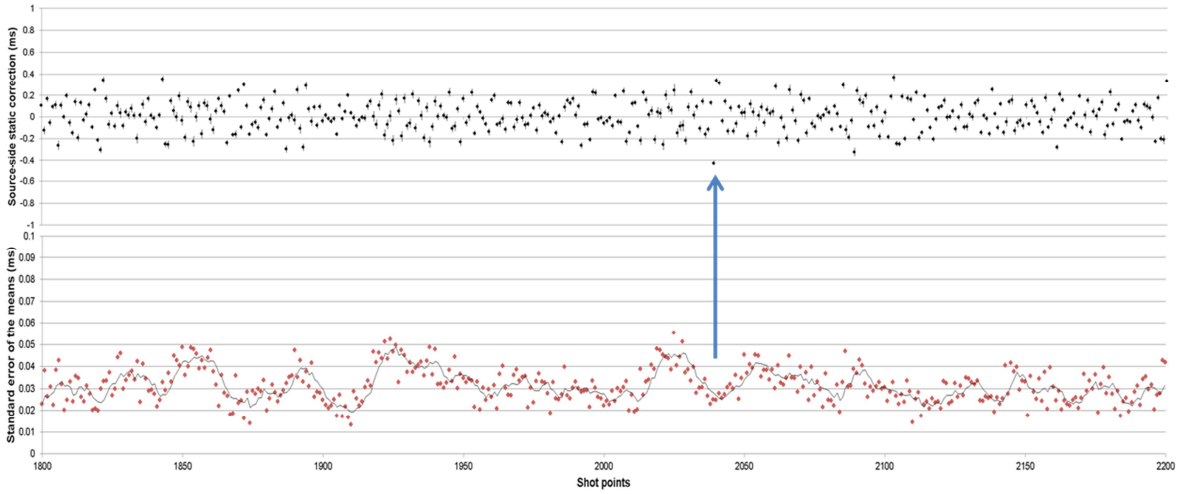

Figure 6: Field data example from 2013 of typical profiles of computed source-side consistent statics with standard error bars (above) and the corresponding standard error for 95% statistical confidence (below) for the first shot consistent linear phase iteration. The arrow highlights the adjacent field shots displayed in the lower half of Figure 5. The statics are distributed Gaussian as expected ($H_s \approx 0.5$m) but the standard errors are not (highlighted by the five point moving average). The variation of the latter is attributed to non-random leakage caused by interplay of environmental and geological variations along the line. Note that the standard error profile is displayed at 10 times exaggeration and is represented as one side of the error bars in the upper profile.

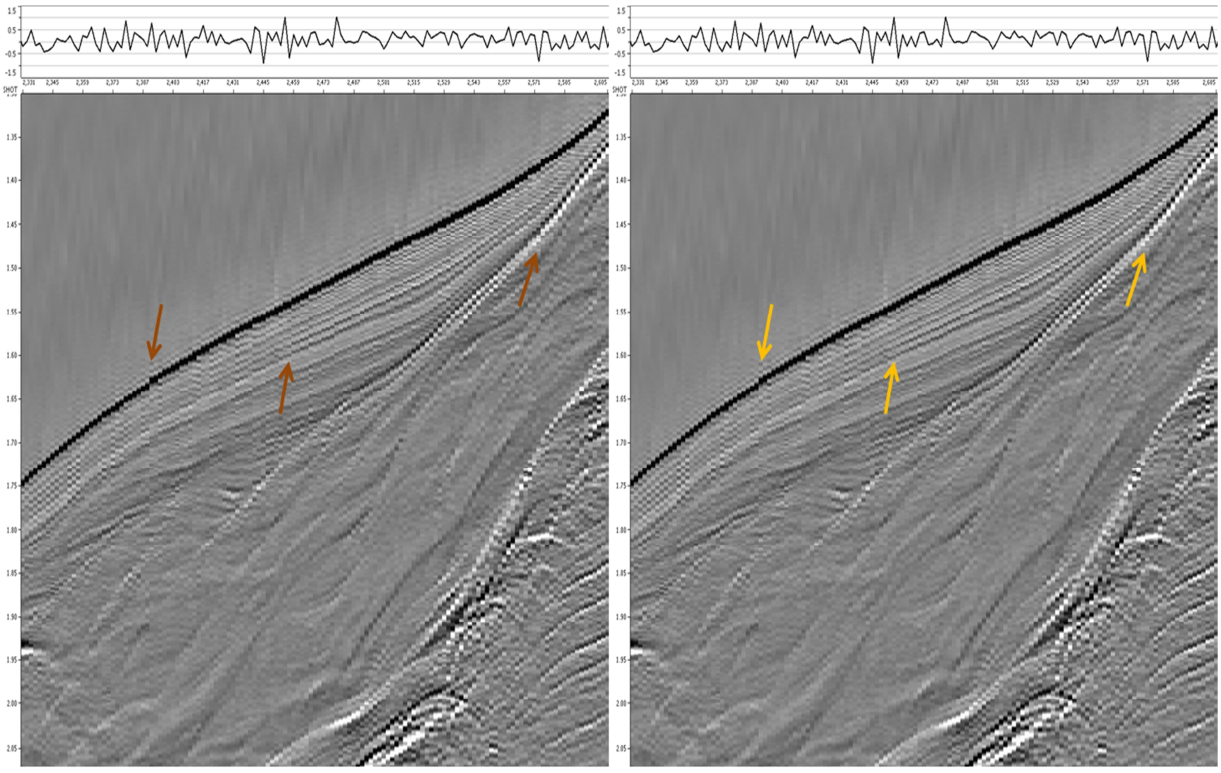

Figure 7: Near trace NMO corrected gather before (left) and after (right) three iterations of the CMP-based shot consistent static correction (profiled above ±1.5ms) for a 2007 field data example ($H_s \approx 3.5$m).

EDITED REFERENCES

Note: This reference list is a copyedited version of the reference list submitted by the author. Reference lists for the 2017 SEG Technical Program Expanded Abstracts have been copyedited so that references provided with the online metadata for each paper will achieve a high degree of linking to cited sources that appear on the Web.

REFERENCES

Brown, E., A. Colling, D. Park, J. Phillips, D. Rothery, and J. Wright, 2006, Waves, tides and shallow-water processes, 2nd ed.: The Open University.

Goto, R. J., E. Kragh, R. Laws, W. G. Morgan, and R. Phillips, 2008, Wave-height-corrected Seismic Data, 70th Annual International Conference and Exhibition, EAGE, Extended Abstracts, https://doi.org/10.3997/2214-4609.20147612.

Lecocq, P., E. Hodges, and M. Sedhom Said, 2014, Correction of sea-surface state: U.S. Patent 61/941, 383.

Manly Hydraulics Laboratory, http://new.mhl.nsw.gov.au/data/realtime/wave/AnalysisAndStatistics.

Meteorological Service Singapore, http://www.weather.gov.sg/weather-marine-waves-height.

Orji, O., W. Söllner, and L. J. Gelius, 2010, Imaging the sea surface using a dual-sensor towed streamer, Geophysics, **75**, no. 6, V111–V118, http://dx.doi.org/10.1190/1.3496439.

Yilmaz, Ö., 2001, Seismic data analysis: SEG, Investigations in Geophysics 10, Volume I, 336–344, https://doi.org/10.1190/1.9781560801580.